BJ www.biochemj.org

BJ Structure

Biochem. J. (2008) **412**, 233–244 (Printed in Great Britain) doi:10.1042/BJ20071443

233

online data

Monitoring conformational changes during the catalytic cycle of OpuAA, the ATPase subunit of the ABC transporter OpuA from *Bacillus subtilis*

Carsten HORN*[1,2], Stefan JENEWEIN*[1], Britta TSCHAPEK*, Werner BOUSCHEN†, Sabine METZGER†, Erhard BREMER‡ and Lutz SCHMITT*[3]

*Institute of Biochemistry, Heinrich Heine University Düsseldorf, Universitätsstr. 1, 40225 Düsseldorf, Germany, †Biological and Medical Research Center, Heinrich Heine University, Düsseldorf, Universitätsstr. 1, 40225 Düsseldorf, Germany, and ‡Laboratory for Microbiology, Department of Biology, Philipps University Marburg, Karl-von-Frisch Str., 35032 Marburg, Germany

The ABC transporter (ATP-binding-cassette transporter) OpuA is one of five membrane transport systems in *Bacillus subtilis* that mediate osmoprotection by importing compatible solutes. Just like all bacterial and archaeal ABC transporters that catalyse the import of substrates, OpuA (where Opu is osmoprotectant uptake) is composed of an ATPase subunit (OpuAA), a transmembrane subunit (OpuAB) and an extracellular substrate-binding protein (OpuAC). In contrast with many well-known ABC-ATPases, OpuAA is composed not only of a catalytic and a helical domain but also of an accessory domain located at its C-terminus. The paradigm of such an architecture is MalK, the ABC-ATPase of the maltose importer of *Escherichia coli*, for which detailed structural and functional information is available. In the present study, we have applied solution FRET (Förster resonance energy transfer) techniques using two single cysteine mutants to obtain initial structural information on the architecture of the OpuAA dimer in solution. Analysing our results in detail and comparing them with the existing MalK structures revealed that the catalytic and helical domains adopted an arrangement similar to those of MalK, whereas profound differences in the three-dimensional orientation of the accessory domain, which contains two CBS (cystathionine β-synthetase) domains, were observed. These results shed new light on the role of this accessory domain present in a certain subset of ABC-ATPase in the fine-tuning of three-dimensional structure and biological function.

Key words: ABC (ATP-binding-cassette)-ATPase, conformational changes, dimer, Förster resonance energy transfer (FRET), osmoprotection.

INTRODUCTION

Osmoregulation is of crucial importance for cell viability and survival [1]. *Bacillus subtilis* has to maintain a cell turgor of approx. 20 bar (1 bar = 100 kPa) [2], which is believed to be the driving force of cell expansion. Thus any change in external osmolarity will induce passive influx (hypo-osmotic stress) or efflux (hyperosmotic stress) of water, thereby changing cell turgor [3,4]. Hyperosmotic conditions (an increase in the extracellular osmolarity) result in the uptake of K^+ ions as a first line of defence to maintain cell turgor in *B. subtilis* [5]. However, the accumulation of a large concentration of a charged ion is detrimental to many cellular functions such as protein function and/or protein–DNA interactions. Thus *B. subtilis* switches to a second line of defence and starts to actively take up or synthesize so-called 'compatible solutes' [6]. In the phyla of bacteria, these 'compatible solutes' are small molecules such as sugars, polyols, amino acids, quaternary amines, sulfate esters or small peptides [7]. The common denominator of all these compounds is the fact that they are highly soluble and bear no net charge under physiological conditions. As a consequence, compatible solutes counteract the deleterious effect of changes in the extracellular osmolarity by equilibrating concentration gradients across the cellular membrane and maintaining cell turgor [4]. In addition to their well-studied role in maintaining an appropriate level of cell water and turgor, compatible solutes also act as protein stabilizers both *in vitro* and *in vivo*. Although the molecular action of compatible solutes as a 'chemical chaperone' is poorly understood, the common opinion is that these molecules act according to the 'volume exclusion model' [8].

Extensive research in the last two decades has identified five transport systems providing osmoprotection in *B. subtilis* through the uptake of compatible solutes [6]. In concert, these five importers allow *B. subtilis* to cope with osmotic stress due to the ability to utilize common compatible solutes such as proline, choline, ectoine, glycine betaine or proline betaine. All of the Opu (osmoprotectant uptake) systems operating in *B. subtilis* belong either to the class of secondary transporters (OpuD and OpuE) or to a subfamily of primary transporters, the ABC (ATP-binding cassette) transporter family (OpuA, OpuB and OpuC; for a recent review see [9]). These membrane transporters ultimately use the energy of ATP for substrate translocation across biological membranes [10]. Although found in all three domains of life and involved in many vital cellular processes, ATP-dependent transporters share a basic blueprint that is composed of four modules: two NBDs (nucleotide-binding domains or subunits) harbouring the ATPase activity and two TMDs (transmembrane domains or subunits) that form the translocation pathway. Next

Abbreviations used: ABC, ATP-binding cassette; CBS, cystathionine β-synthetase; CFTR, cystic fibrosis transmembrane conductance regulator; ESI, electrospray ionization; FRET, Förster resonance energy transfer; IMPDH, inosine-monophosphate dehydrogenase; MalK, maltose import system; NBD, nucleotide-binding domain; OG, Oregon Green® 488 maleinimide; Opu, osmoprotectant uptake; rmsd, root mean square deviation; SBP, substrate-binding protein; SEC, size-exclusion chromatography; TMD, transmembrane domain; TR, Texas Red® C2 maleinimide.

[1] These authors contributed equally to the present study.

[2] Present address: CellGenix Technology Transfer GmbH, Am Flughafen 16, 79108 Freiburg, Germany

[3] To whom correspondence should be addressed (email lutz.schmitt@uni-duesseldorf.de).

to the substrate, ABC transporters can be classified by the directionality of transport: import or export. OpuA belongs to the family of ABC importers, since it catalyses the import of glycine betaine and proline betaine from the extracellular medium into the bacterial cytosol. Additionally to the NBD (OpuAA) [11] and the TMD (OpuAB) [9], this family always requires another component for functionality: a so-called SBP (substrate-binding protein; OpuAC in the case of the OpuA transporter [12]). Recent insights into the molecular function of these ABC transporters were provided by X-ray crystallography that determined the high-resolution structures of isolated NBDs (for a recent review see [13]) and intact ABC transporters [14–19]. For example, crystal structures of the NBD of the maltose import system (MalK) in the nucleotide-free, ATP- and ADP-bound states have deciphered many of the molecular principles that govern ATP binding and hydrolysis and have resulted in the proposal of a 'tweezer-like motion' that accompanies maltose import [20,21].

OpuAA, the NBD of the OpuA transporter, and MalK, the NBD of the maltose importer, share interesting similarities. Both NBDs not only are composed of a catalytic and a helical domain that harbours all conserved sequence motifs of these ATPases such as the Walker A and B motifs and the hallmark of ABC transporters, the C-loop or ABC-signature motif [10], but also contain an accessory domain, which is composed of approx. 150 amino acids and is located C-terminal to the canonical NBD (catalytic and helical domain). In the case of MalK, this accessory domain interacts with at least two enzymes, MalT [22] and enzyme IIA [23], thereby regulating the expression of the maltose operon. Furthermore, in the 'tweezer-like motion' model, the accessory domains act as the bottom of tweezers keeping two NBDs together during a catalytic cycle, whereas the canonical part (the catalytic and helical domains) undergoes ATP-induced dimerization remaining monomeric in the nucleotide-free and ADP-bound states.

Biochemical studies have established that OpuAA undergoes a dynamic monomer–dimer equilibrium and forms dimers in the nucleotide-free and ATP-bound states but, in striking contrast with MalK, becomes monomeric in the ADP-bound state [11]. The closely related OpuA glycine betaine importer in *Lactococcus lactis* has been intensively studied in the past by biochemical approaches [24]. Like OpuAA from *B. subtilis*, the NBD of the *L. lactis* homologue is composed of a canonical part (catalytic and helical domain) and an accessory domain. Most important was the fact that the accessory domain contains the fingerprint of two CBS (cystathionine β-synthetase) domains [25] and is involved in sensing osmotic stress signals that activate the transport function of the *L. lactis* OpuA system [26].

In the present study, we have applied FRET (Förster resonance energy transfer) studies to analyse the structure of OpuAA in solution by monitoring and determining the conformational changes taking place during the catalytic cycle of the ATPase. After generating suitable single cysteine mutants of OpuAA, static and time-resolved FRET measurements provided a set of distance restrains that were employed to model the overall structures of OpuAA in the nucleotide-free, ATP- and ADP-bound states based on the available crystal structures of MalK [20,21]. Surprisingly, the three-dimensional positioning of the accessory domains with respect to the canonical part of the NBD was different, whereas the overall conformational changes during the catalytic cycle were identical with the ones determined previously for other isolated NBDs [20,27–29]. Thus our results provide novel insights on the architecture of OpuAA from *B. subtilis* and suggest that the accessory domains play an important role in the structural and functional regulation of these proteins.

MATERIALS AND METHODS

Cloning, expression and isolation of OpuAA single cysteine mutants and the F19W mutant

To change native amino acids to cysteine, 5′ and 3′ fragments were amplified by PCR using pBAD33/OpuAA as a template and flanking/mutagenic primer pairs as follows: S45C, 5′ CH7/CH29 and 3′ CH8/CH28; G161C, 5′ CH7/CH41 and 3′ CH8/CH40; F19W, CH47/CH48. The primers are CH7, 5′-GGAATTCCATATGAGTGTAGATGAGAAACCAATTA-3′; CH8, 5′-ATATATAAAGCTTATTAGTGATGGTGATGGTGATGTTCACCTCCTGTGCAGAAGGATCTTG-3′; CH28, 5′-ATTAACCCCAACGGTACATCCGGTTGCTTTCAG-3′; CH29, 5′-CTGAAAGCAACCGGATGTACCGTTGGGGTTAAT-3′; CH40, 5′-ATATTGGTGTTCAAAACATTCCAGTGGAACGAG-3′; CH41, 5′-CTCGTTGGACTGGAATGTTTTGAACACCAATAT-3′; CH47, 5′-ATTCTTTGTTTGTTTCCCCCAAATCTTAGAGAC-3′; and CH48, 5′-GTCTCTAAGATTTGGGGGAAACAAACAAAGAAG-3′. Secondly, the mutated *opuAA* gene was amplified using both overlapping fragments as a template and the flanking primers CH7 and CH8. The PCR products were digested with NdeI/HindIII (New England Biolabs) and cloned into pBAD33. All gene inserts were sequenced according to the ddNTP method and were free of mutations. Mutant proteins were produced in *Escherichia coli* and purified by IMAC (immobilized metal-ion-affinity chromatography) as described previously [11]. Monomeric OpuAA was isolated by SEC (size-exclusion chromatography) using a Superdex200 HR 26/60 column (GE Healthcare) equilibrated with buffer A [10 mM sodium phosphate and 0.1 mM EDTA (pH 7.5)] supplemented with 1 M NaCl. Protein-containing fractions were pooled and stored at 4 °C until further use.

ATPase activity assays

ATPase activity of monomeric OpuAA was analysed by an enzyme-linked assay as described previously [11] in 10 mM sodium phosphate buffer (pH 7.5) and 1 M NaCl. In brief, absorbance at 340 nm was monitored at 1 min time intervals over a period of 15 min at 22 ± 2 °C. Data points of the whole measuring period or until all NADH was consumed (over a period of at least 7 min) were used to calculate linear slopes $\Delta A/\Delta t_{\mathrm{OpuAA}}$. To account for autohydrolysis of ATP, similar assays were performed in the absence of OpuAA. After background subtraction ($\Delta\Delta A/\Delta\Delta t = \Delta A/\Delta t_{\mathrm{OpuAA}} - \Delta A/\Delta t_{\mathrm{buffer}}$) reaction velocities were calculated according to eqn (1):

$$v = \frac{\Delta\Delta A}{\Delta\Delta t} \cdot \frac{1}{2590\ \mathrm{M}^{-1} \cdot c_0} \quad (1)$$

In this equation, v is the reaction velocity, $\Delta\Delta A/\Delta\Delta t$ denotes the linear slopes of the time-dependent decay of NADH absorbance at 340 nm of OpuAA samples after background subtraction, and c_0 is the final concentration of OpuAA. Reaction velocities represent the average value of two independent measurements.

Fluorophore labelling of OpuAA mutants

For site-specific labelling of mutant OpuAA with fluorophore dyes, cysteine-specific maleinimide chemistry was used. Typically, OpuAA was passed over a PD-10 colum (GE Healthcare) to remove DTT (dithiothreitol) that was added to prevent disulfide bond formation during storage and mixed at a concentration of 10 μM with 25 μM dye [donor dye: OG (Oregon Green® 488 maleinimide; Molecular Probes), 20 mM in dimethylformamide; acceptor dye: TR (Texas Red® C2 maleinimide;

Molecular Probes), 4.1 mM in methanol] and incubated overnight at 4 °C. Protein and free dye were separated using a PD-10 column (GE Healthcare) equilibrated with buffer A supplemented with 10 mM NaCl. To isolate the labelled mutants in a quantitative fashion, anion-exchange chromatography was used to separate labelled and non-labelled OpuAA. After sample loading on to a 1 ml Q-Sepharose HiTrap column (GE Healthcare) equilibrated with buffer A supplemented with 10 mM NaCl, a 12 column volume gradient (0.01–2.5 M NaCl in buffer A) was applied. Elution was followed at 216 nm, 491 nm and 592 nm respectively.

Labelling efficiency and protein concentration

Protein concentration was determined using the BCA (bicinchoninic acid) assay following the procedure provided by the manufacturer (Pierce) using BSA as a standard. To determine the efficiency of fluorophore labelling, the molar absorption coefficient of the isolated dyes was used as provided by the manufacture (Molecular Probes). However, not only incomplete labelling was evident but also a blue shift of the emission maximum as well as changes in the molar absorption coefficient (up to 2-fold; see Supplementary Figure S2 at http://www.BiochemJ.org/bj/412/bj4120233add.htm). Thus an additional purification step to quantitatively separate labelled and non-labelled protein was employed (see above) to circumvent these problems and avoid spectroscopic determination of the labelling efficiency.

MS

Samples obtained from anion-exchange chromatography (OpuAA S45C–OG or OpuAA S45C–TR) or purified OpuAA S45C were desalted over a C_{18} reversed-phase minicolumn (perfect pure C_{18}; Eppendorf) before mass spectrometric analysis. ESI (electrospray ionization)–MS measurements were performed using a ESI-QqTOF instrument (QSTAR XL, Applied Biosystems) equipped with a nanospray ionsource. The ESI–MS spectra were reconstructed using the deconvolution algorithm included in the analyst software (Applied Biosystems).

FRET sample preparation

To measure FRET efficiencies within homodimeric OpuAA, all donors had to be paired with acceptors in the assembled dimer. Therefore OpuAA–TR and OpuAA–OG were mixed in a 9:1 molar ratio. In brief, species were mixed at conditions of dynamic monomer/dimer equilibrium (buffer A + 100 mM NaCl) and concentrated to 30 μM to force dimer formation. After incubation overnight at 4 °C, samples were applied to a Superdex200 HR 10/30 SEC column (GE Healthcare) previously equilibrated with buffer A supplemented with 1 M NaCl to isolate the dimeric species. The dimer fraction was used for the FRET assay, whereas the monomer fraction was used only for control experiments. For ADP/Mg^{2+}-mediated decay the dimer fraction was diluted into buffer A + 100 mM NaCl.

FRET assays

Fluorescence was measured with a Cary-Eclipse spectrometer (Varian) at a λ_{ex} of 492 nm at a temperature (T) of 20 ± 1 °C and a slit width of 5nm in 10 mM sodium phosphate (pH 7.5), 0.1 mM EDTA and 1 M NaCl. In static FRET assays, samples were separately analysed with emission recording from 500 to 650 nm and analysed according to eqn (2) [30]:

$$E_T = \frac{R_0^6}{R_0^6 + R^6} \quad (2)$$

In time-resolved FRET assays, the sample was chased with 10 mM ADP or ADP/Mg^{2+} (pH 7.5) at $t = 0$ to allow dimer dissociation. Fluorescence at time t (F_t) was followed at 519 nm over a period of 3600 s at 5 s intervals and fitted to eqn (3). In this case, fitting parameters were: fluorescence at $t = 0$ ($F_{t=0}$), fluorescence increase at infinite time (ΔF) and half-time (τ).

$$F_t = F_{t=0} + \Delta F \cdot (1 - e^{-t/\tau}) \quad (3)$$

Amplitudes were used to calculate the E_T-time-course according to eqn (4). For $t = 0$ the E_T value for the original, nucleotide-free state was extrapolated and using the Förster-distance [$R_0 = 51$ Å (1 Å = 0.1 nm) for the OG–TR pair] of this donor/acceptor pair, its distance in this state was calculated.

$$E_T(t) = 1 - \frac{F_t}{F_{t=0} + \Delta F} = 1 - \frac{F_t}{F_{t=\infty}} = \frac{R_0^6}{R_0^6 + R(t)^6} \quad (4)$$

Intrinsic tryptophan fluorescence measurements of the F19W mutant of OpuAA

All measurements were performed at 22 ± 1 °C on a Cary-Eclipse spectrophotometer employing a slit width of 5 nm. Wild-type OpuAA does not contain any tryptophan residues. The tryptophan residue engineered at position 19 of OpuAA was excited at 290 nm, and fluorescence was collected at the emission maximum (350 nm) at a protein concentration of 2 μM dimeric OpuAA in 10 mM sodium phosphate (pH 7.5), 1 M NaCl and 0.1 mM EDTA. The chase was started by adding 1 mM ADP and 5 mM Mg^{2+}. Data were analysed using a single exponential decay.

Molecular modelling and structural analysis

Molecular modelling was performed with MODELLER 9v1 [31] employing standard settings. As templates, the crystal structures of MalK in the semi-open, nucleotide-free (PDB entry: 1Q1B), the open nucleotide-free (PDB entry: 1Q1E), the ATP- (PDB entry: 1Q12) and ADP-bound (PDB entry: 1AWN) states were used. The quality of the obtained structural models of OpuAA in the corresponding functional states was verified with PROCHECK [32] and compared with the template structure. The initial models were further modified in O after imposing the FRET-derived distance restrains using sgFRET (http://www.mpibpc.mpg.de/groups/grubmueller/start/software/fretsg-1.0/fretsg.html). Structural superimpositions were performed using LSQMAN [33] using the indicated motifs as anchor points. The buried surface areas were calculated using areaimol of the CCP4 suite [33a]. All structural figures were prepared using PyMol (http://www.pymol.org).

RESULTS

Biochemical studies have demonstrated that OpuAA from *B. subtilis* undergoes a dynamic monomer–dimer equilibrium [11]. Interestingly, this equilibrium depends on the presence or absence of nucleotides. To gain further insights into the underlying conformational changes, we applied FRET techniques of single cysteine mutants of OpuAA in solution. Since the crystal structures of MalK from *E. coli* are available in the nucleotide-free and ATP- and ADP-bound states [20,21], they provide a lead structure (homology of 69 %) for OpuAA homology modelling and would open up the possibility to translate the distance restrains derived from FRET measurements into a three-dimensional model of OpuAA. A homology model of OpuAA using the crystal structure of MalK in the nucleotide-free state (PDB entry: 1Q1B)

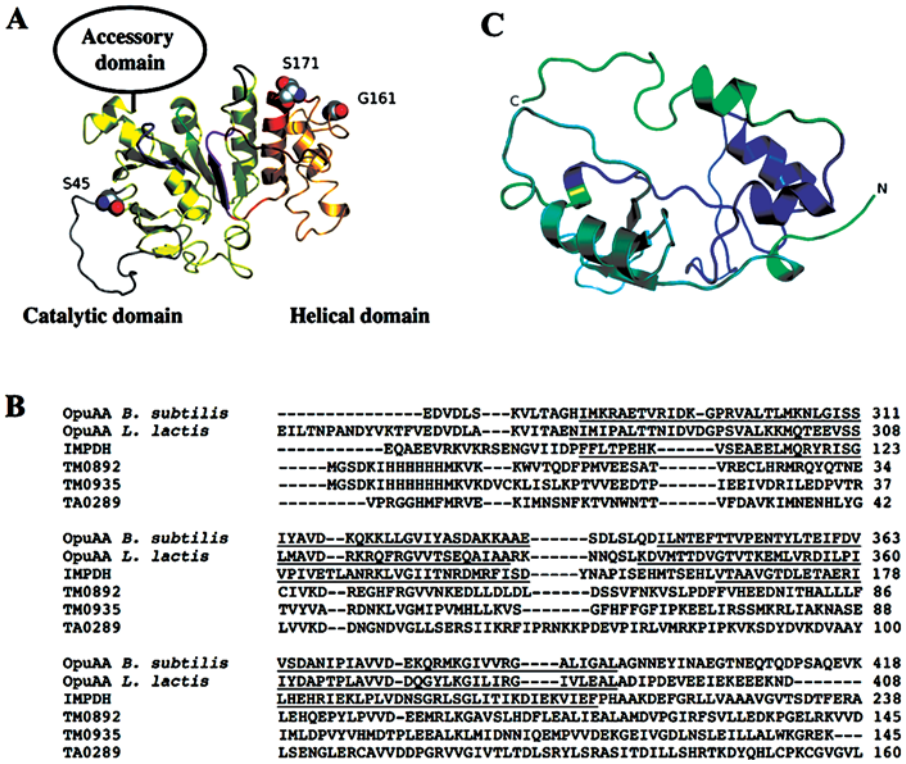

Figure 1 Homology model of OpuAA

(**A**) Homology model of the core domain OpuAA in the nucleotide-free state lacking the accessory domain. The model was generated using MODELLER 9v1 [31] as described in the Materials and methods section. The helical domain is shown in light tan and the catalytic domain in yellow. The OpuAA-specific insertion between β-strands 1 and 2 is highlighted in grey. Conserved motifs are colour-coded as follows: Walker A motif (blue), C-loop or ABC-signature motif (red), Walker B motif (magenta), D-loop (black) and H-loop (green). Positions of the single cysteine mutants are highlighted as spheres and labelled. (**B**) Sequence alignment of the accessory domains of OpuAA from *B. subtilis* (residues 277–418) and *L. lactis* (residues 271–408) containing a tandem CBS domain (residues 283–335 and 342–394 in the case of OpuAA from *B. subtilis*) with selected proteins containing CBS domains, for which a crystal structure is available. The two CBS domains in OpuAA from *B. subtilis* and *L. lactis* and IMPDH [41] are underlined. TM0892, open reading frame 0892 from *Thermotoga maritima* with unknown function (PDB entry: 1VR9); TM0935, open reading frame 0935 from *T. maritima* with unknown function (PDB entry: 1O50); TA0289, open reading frame 0289 from *Thermoplasma acidophilum* with unknown function (PDB entry: 1PVM). (**C**) Homology model of the accessory domain of OpuAA from *B. subtilis*. The tandem CBS domains are coloured cyan (CBS1) and blue (CBS2) respectively. The N- and C-termini, residues 277 and 418 respectively, of OpuAA are indicated. The model was derived from the crystal structure of TA0289 (PDB entry: 1PVM) due to the high sequence identity (25 % identity and 51 % homology) and obtained as described in the Materials and methods section.

was generated. As shown in Figure 1(A), OpuAA indeed adopts a 'MalK-like' structure [20] composed of a helical (coloured tan) and a catalytic (coloured yellow) domain. The catalytic domain of OpuAA contains a 24-amino-acid insertion between β-strands 1 and 2 (highlighted in grey), which is not present in other ABC domains. However, homology modelling of the accessory domain (represented by a circle in Figure 1A) was not straightforward. In clear contrast with MalK, the primary structure of OpuAA does not contain the fingerprint of the CUT1 (carbohydrate uptake transporter 1) subfamily represented by a characteristic GI/VRPE consensus sequence [34]. Rather the sequence indicates the presence of two CBS domains (Figure 1B) as evident by a sequence alignment of the accessory domain of OpuAA from *B. subtilis* with OpuAA from *L. lactis*, IMPDH (inosine-monophosphate dehydrogenase) and the orphan open reading frames from *Thermotoga maritimus* and *Thermoplasma acidophilum* [25]. These open reading frames were chosen, because crystal structures of the CBS modules are available (see the Figure legends for the corresponding PDB entries). Among the four crystal structures, *T. acidophilum* TA0289 had the highest sequence similarity (51 %) and was used for separate homology modelling. The resulting model of the isolated accessory domain of OpuAA is shown in Figure 1(C) displaying the characteristics of the tandem organization of CBS domains. Since no prior information of the relative orientation of the accessory and the core NBD domain are available, no attempts were made to include the homology model of the CBS domain of OpuAA (Figure 1C) into the MalK-derived homology model of OpuAA (Figure 1A).

With the homology model at hand, we selected three residues of OpuAA within the catalytic and helical domains for changing to a cysteine residue. These residues are highlighted as spheres in Figure 1(A). Ser^{45} is located in the catalytic domain at the C-terminal end of the OpuAA-specific insertion between β-strands 1 and 2. Gly^{161} is at the N-terminal end of the ABC-signature motif. Ser^{171}, the conserved serine residue of the ABC-signature motif, was also selected for cysteine mutation to distinguish the composite dimer architecture from the one observed in the MalK crystal structure from *Thermococcus litoralis* [35], which shows a different arrangement of the two monomers in the NBD-dimer. Wild-type OpuAA and the three cysteine mutants were overexpressed in *E. coli* and purified as described in the Materials and methods section. Analysis of the two single cysteine mutants (S45C and G161C) under reducing and oxidizing conditions (see Supplementary Figure S1 at http://www.BiochemJ.org/bj/412/bj4120233add.htm) demonstrated that only negligible intermolecular disulfide bond formation occurred. More importantly for our conformational

Table 1 Kinetic parameters of monomeric OpuAA and the mutants used in the present study

ATPase assays were performed in 10 mM sodium phosphate (pH 7.5) and 1 M NaCl as described in the Materials and methods section. Values are means ± S.D. of two independent measurements.

Protein	K_m (mM)	k_{cat} (ATP/min)	Catalytic efficiency ($M^{-1} \cdot min^{-1}$)
OpuAA	0.6 ± 0.2	1.1 ± 0.1	1833
OpuAA S45C	0.7 ± 0.1	1.3 ± 0.1	1857
OpuAA G161C	2.8 ± 0.4	0.8 ± 0.1	285
OpuAA S171C	Not determined	0.08 ± 0.01	Not calculated
OpuAA F19W	1.7 ± 0.1	1.5 ± 0.1	882

analysis was the ATPase activity of the mutant proteins (Table 1). The wild-type enzyme hydrolysed ATP at a rate of 1.1 ± 0.1 min^{-1} under the conditions of the assay [11]. In contrast with the S45C and the G161C mutants, which hydrolysed ATP at comparable rates, the S171C mutant displayed hardly any turnover (0.08 ± 0.01 min^{-1}). Owing to this result, the S171C mutant was not used for further studies.

In order to use FRET quantitatively and to extract distance information, it is of importance to obtain a reliable value for the labelling efficiency [36]. The engineered single cysteine mutants of OpuAA allowed us to employ maleimide chemistry and covalently link the individual fluorophores, OG or TR. Surprisingly, labelling efficiencies were rather low (approx. 50 % for the G161C and approx. 60 % for the S45C mutant for both dyes). To exclude non-specific labelling due to the prolonged reaction time, wild-type OpuAA was treated with the fluorophores under similar conditions. Here, no labelling above background was detected after separating protein and fluorophore (results not shown). Additionally, attachment of the dyes changed their molar absorption coefficient as well as the absorption maximum (12 nm for TR and 8 nm for OR; Supplementary Figure S2). To account for the low labelling efficiency and the changes in the physical properties of the protein-attached fluorophores, we established a second purification step, anion-exchange chromatography, to separate labelled and non-labelled protein (Figure 2). A separation of a labelled and a non-labelled protein species is evident from the absorption properties shown in the representative chromatograms of OpuAA S45C–OG (Figure 2A), OpuAA S45C–TR (Figure 2B), OpuAA G161C–OG (Figure 2C) and OpuAA G161C–TR (Figure 2D).

To investigate further whether the apparent separation was indeed quantitative, we applied ESI–MS of the two fractions obtained by anion-exchange chromatography. ESI–MS analysis of fraction I, which eluted at lower ionic strength, revealed the presence of a single protein species with a molecular mass of 47 174 Da (Figure 3A). The calculated average molecular mass of OpuAA S45C, including a C-terminal hexahistidine tag and a formylated methionine residue, is 47 174.48 Da. The second fraction, which eluted at higher ionic strength, revealed the presence of a single protein species of 47 657 Da in the case of OpuAA S45C–OG (Figure 3B) and 47 921 Da in the case of OpuAA S45C–TR (Figure 3C). These mass differences correspond within experimental error of the MS measurements to the molecular masses of the individual fluorophores [differences of 483 Da for the sodium adduct of OG (expected 486.35 Da) and 747 Da for the sodium adduct of TR (expected 751.83 Da)].

A detailed analysis of the monomer–dimer equilibrium of OpuAA [11], has provided a toolbox to generate monomers or dimers of OpuAA depending on the protein concentration and ionic strength. This allowed us to prepare OpuAA–OG/OpuAA–TR pairs at a molar ratio of 1:9, which ensures that all (>95 %) OG-labelled OpuAA molecules are indeed in an OG–TR dimer.

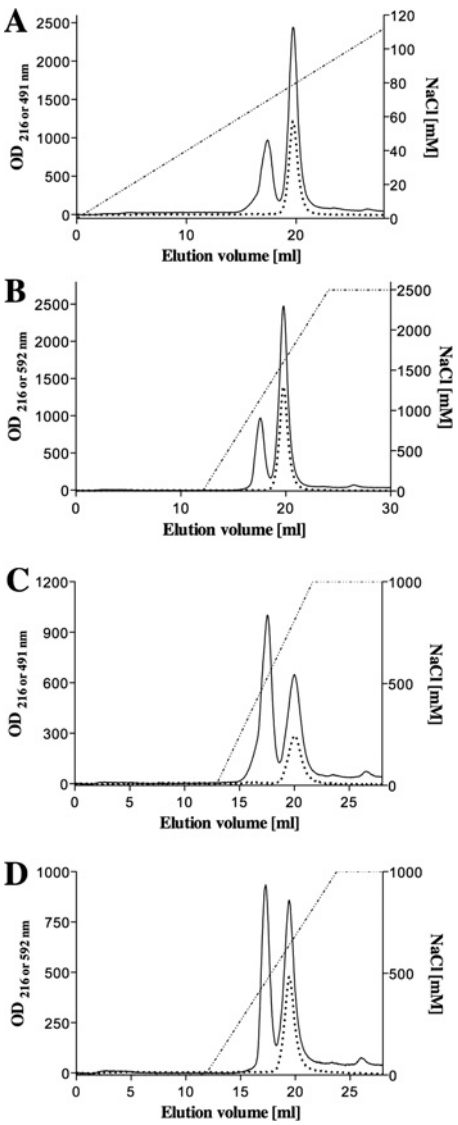

Figure 2 Quantitative separation of labelled and non-labelled single cysteine mutants of OpuAA by anion-exchange chromatography

A (OD) at 216 nm (protein absorption) is shown as a solid line and *A* at 491 nm (OG absorption; **A** and **C**) and 591 nm (TR absorption; **B** and **D**) is shown as dotted lines respectively. The applied NaCl concentration gradient is shown as a dashed line in the indicated concentration range. (**A**) OpuAA S45C–OG, (**B**) OpuAA S45C–TR, (**C**) OpuAA G161C–OG and (**D**) OpuAA G161C–TR. For further details see the Materials and methods section.

On the other hand, a high molar excess of acceptor might result in an apparent increase in transfer efficiency due to radiation-dependent processes such as acceptor self-absorption.

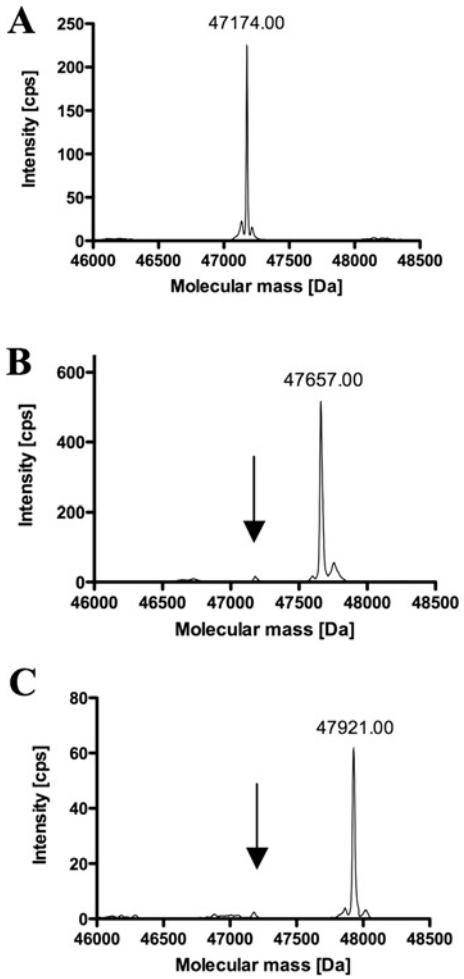

Figure 3 High-resolution MS analysis of OpuAA (A), OpuAA S45C–OG (B) and OpuAA S45C–TR (C)

The arrow in (**B**) and (**C**) indicates the position of unlabelled OpuAA, which is below 2% according to an analysis of the peak area.

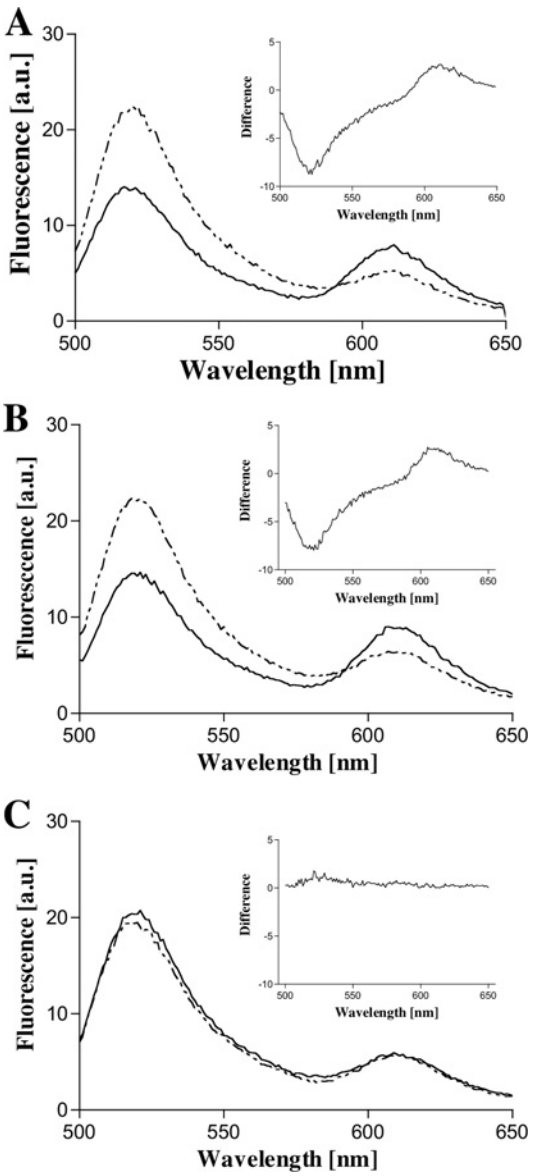

Figure 4 Static FRET measurements of OpuAA S45C in the nucleotide-free (A), ATP-bound (B) and ADP-bound (C) states in the absence of Mg^{2+}

In all three panels, the broken line represents the sum of two individual FRET experiments, OpuAA S45C–OG/OpuAA wild-type (molar ratio of 1:9) and wild-type OpuAA/OpuAA S45C-TR (molar ratio 1:9). The solid line shows the actual FRET experiments of OpuAA S45C–OG/OpuAA S45C–TR (molar ratio of 1:9). Acceptor concentration was always kept at 50 nM, and the corresponding dimers were prepared as described in the Materials and methods section. The inset in each panel shows the difference spectra of the corresponding FRET experiments (OG and TR pairs). The buffer used was 10 mM sodium phosphate (pH 7.5), 0.1 mM EDTA and 1 M NaCl. a.u., absorbance units.

However, these processes depend solely on the concentration of the acceptor and a proper choice will eliminate this obstacle. Therefore we measured the fluorescence of a 50 nM sample of OpuAA–OG (donor) in the presence or absence of a 9-fold molar excess of TR-conjugated OpuAA (results not shown) under conditions that abolish FRET. Comparison of the two spectra clearly showed that marginal self-absorption of TR occurred. Consequently, we used a fixed donor concentration of 50 nM in all subsequent experiments.

A representative set of static FRET experiments is shown in Figure 4 for the OpuAA S45C–OG/OpuAA S45C–TR dimer in the nucleotide-free (Figure 4A), the ATP-bound (Figure 4B) and the ADP-bound (Figure 4C) states. The broken lines show the sum of two control experiments, OpuAA S45C–OG and wild-type OpuAA (molar ratio of 1:9) and wild-type OpuAA and OpuAA S45C–TR (molar ratio of 1:9), whereas the solid lines show the fluorescence spectrum of an OpuAA S45C–OG/OpuAA S45C–TR mixture (molar ratio of 1:9). The insets show the corresponding difference spectra. As is evident from these experiments, FRET can be detected for the nucleotide-free and the ATP-bound states of dimeric OpuAA, but not for the ADP-bound state. The FRET efficiencies were calculated to 34% and 39% for the nucleotide-free and ATP-bound state according to eqn (2). A summary of the FRET efficiencies determined for this and the other combinations is given in Table 2.

Distance determinations through static FRET experiments require an accurate knowledge of the protein concentration. In the present study, concentration determination was complicated by the fact that the molar absorption coefficients of the dyes changed upon covalent attachment to the protein (see Supplementary Figure S2). We determined protein concentrations as outlined in the Materials and methods section and incorporated the changed molar absorption coefficients determined under the experimental conditions, but any error in the determination would

Table 2 Summary of the static and time-resolved FRET experiments

The dimeric species of the indicated single cysteine mutants of OpuAA of the nucleotide-free and ATP-bound states and the monomeric species of the indicated single cysteine mutants of OpuAA in the ADP-bound state were analysed as described in the Materials and methods section in the absence of Mg^{2+}. The determined transfer efficiencies at 519 nm (donor emission maximum) or the static FRET experiments were translated in distances according to the Förster equation assuming a Förster radius of the OG/TR pair of 51 Å [30]. In the case of the time-resolved experiments, amplitudes and half times were calculated from the ADP/Mg^{2+}-induced decay of the dimeric forms of labelled OpuAA mutants as described in the Materials and methods section.

	Static FRET					Time-resolved FRET		
	Nucleotide free		ATP			Nucleotide-free		
Dimer species	Transfer efficiency (%)	Distance (Å)	Transfer efficiency (%)	Distance (Å)	ADP/Mg^{2+}	Half time (min)	Transfer efficiency (%)	Distance (Å)
S45C–S45C	34	57	39	55	No transfer	22 ± 0.3	33	59
S45C–G161C	47	52	79	41	No transfer	20.7 ± 0.1	47	52
G161C–G161C	49	51	65	46	No transfer	12.9 ± 0.1	49	51

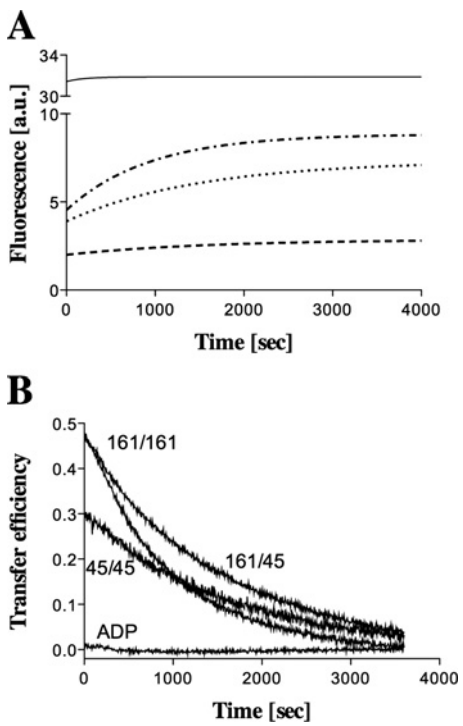

Figure 5 Time-resolved FRET experiments

(**A**) Dimers of the nucleotide-free state were prepared as described in the Materials and methods section and were chased by the addition of 10 mM ADP/Mg^{2+}. Fluorescence was measured at 519 nm in 5 s intervals. From bottom to top: dimeric OpuAA S45C–OG/OpuAA S45C–TR (dashed line), dimeric OpuAA G161C–OG/OpuAA S45C–TR (dotted line), dimeric OpuAA G161C–OG/OpuAA G161C–TR (dotted-dashed line) and monomeric OpuAA G161C–OG/OpuAA G161C–TR (solid line). Note that monomeric samples were measured at an approx. 4-fold higher concentration than the dimeric samples. Traces were analysed according to eqn (3). The buffer used was 10 mM sodium phosphate (pH 7.5), 0.1 mM EDTA and 1 M NaCl. (**B**) Time-resolved transfer efficiencies were calculated according to eqn (4) and extrapolated to $t = 0$ to determine the initial transfer efficiencies, which are summarized in Table 2. a.u., absorbance units.

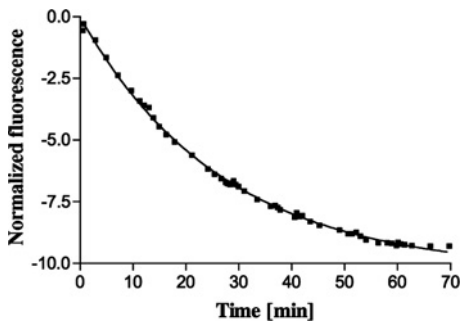

Figure 6 Time-resolved intrinsic tryptophan fluorescence of the OpuAA F19W mutant

The nucleotide-free dimeric form of OpuAA was prepared as described for the wild-type ATPase and ADP (1 mM) was added at zero time in the absence of Mg^{2+}. Tryptophan fluorescence was monitored at 350 nm over the indicated time frame and evaluated as described in the Materials and methods section. The buffer used was 10 mM sodium phosphate (pH 7.5), 0.1 mM EDTA and 1 M NaCl.

drastically affect the FRET distances extracted from those measurements. Thus we also thought of establishing an experimental approach that was independent of a prior exact knowledge of protein concentration. Here, time-resolved changes in donor fluorescence of monomeric or dimeric OpuAA G161C–OG/OpuAA G161C–TR, dimeric OpuAA G161C–OG/OpuAA S45C–TR and dimeric OpuAA S45C–OG/OpuAA S45C–TR (Figure 5A) provided a tool to countercheck the distance information of the static FRET experiments and to validate these results. Nucleotide-free samples of the indicated combinations were incubated with ADP/Mg^{2+}, and fluorescence was measured over the indicated time frame. The observed donor fluorescence increased over time in a strictly mono-exponential fashion for all dimeric probes, although it remained constant for the monomeric probe. Thus the increase in donor fluorescence corresponds to dimer decay, and the decay reaction was evaluated according to eqn (3). This analysis provided the amplitudes and half times of dimer decay and could be used to calculate the transfer efficiency for the individual combinations according to eqn (4) by extrapolation of the data to $t = 0$ (Figure 5B). This extrapolation allowed us to extract the transfer efficiencies without prior knowledge of protein concentration or the exact starting time point of the experiment. A summary of the calculated values is given in Table 2. This demonstrates the agreement between transfer efficiencies determined by static and time-resolved FRET.

Additional support for the ADP-induced dimer decay comes from independent experiments using the F19W mutant of OpuAA (Figure 6). Phe[19], which based on sequence comparisons is interacting with bound nucleotide via π–π stacking, was mutated to a tryptophan residue to use intrinsic tryptophan fluorescence quenching to monitor nucleotide association and dissociation similar to the approach employed for the isolated NBD of HlyB [37]. Kinetic parameters of this mutant are summarized in Table 1. As shown in Figure 6, chasing of dimeric nucleotide-free OpuAA with ADP resulted in a quenching of the detected tryptophan fluorescence. As analysed for the monomeric form of OpuAA, the observed fluorescence reduction

is due to nucleotide binding and π–π interaction of the adenine moiety of ADP or ATP and Trp[19] (Supplementary Figure S3 at http://www.BiochemJ.org/bj/412/bj4120233add.htm). However, the determined half time of fluorescence decay (18 ± 4 min) is similiar with the half times determined for the time-resolved fluorescence experiments within experimental error (Table 3).

Based on the FRET-derived distance information for the two homo-pairs (S45C/S45C and G161C/G161C) and the hetero-pair (S45C/G161C) in the nucleotide-free and ATP-bound state (Table 2), a molecular model was created using FRETsg as anchor points for a structural alignment in O [38]. Although the Cα–Cα distances obtained from the FRET studies of the homo-pairs [56.9 Å (45–45) and 51.3 Å (161–161)] agreed with the open conformation of MalK (59.9 Å and 51.9 Å respectively) [20], the distance of the S45C/G161C pair was approx. twice the distance measured in MalK (52.1 Å compared with 22.3 Å). Thus the open nucleotide-free dimer of MalK was adjusted accordingly. Here, one monomer was kept fixed while the other was treated as a rigid body. The resulting model for OpuAA satisfying all FRET-derived distance restrains is shown in Figure 7(A). The canonical part of each NBD monomer, composed of the catalytic and helical subdomains, is shown in yellow and light orange respectively, and the accessory domains are in grey. The Walker A and ABC-signature motifs are highlighted in blue and red respectively, whereas the Cα trace of the amino acids, which were mutated to cysteine residues and labelled with the corresponding fluorophores, is coloured green (position 45) and dark grey (position 161). Thin broken lines indicate the distances between the labelled amino acids, which were calculated from the FRET measurements. Interestingly, the closest Cα–Cα distance between opposing Walker A and ABC-signature motifs are 17 and 20 Å respectively. These values agree with the distance determined for the corresponding Cα atoms of the nucleotide-free open form of MalK (17 Å) from *E. coli* [20]. Thus it appears that the overall structure of the canonical part of the NBD is identical between OpuAA and MalK. However, the accessory domains are in a different orientation from that expected from the MalK structure. As a consequence, severe clashes occur between the canonical and accessory part of opposing OpuAA monomers (Figure 7A), indicating that the accessory domain has to adopt a different orientation. Furthermore, the D-loop motifs (SALD in OpuAA and SNLD in MalK) of opposing monomers are in close contact (Cα–Cα distance of 7 Å). As shown in Figure 7(B), structural superimposition reveals that one monomer of the OpuAA model aligns very well with a monomer of the nucleotide-free open structure of MalK [rmsd (root mean square deviation) of 1 Å over 381 Cα atoms]. The two monomers of MalK are coloured magenta and cyan and the Walker A and ABC-signature motifs in blue and red respectively. In clear contrast, the second monomer displayed a translational movement of 9.5 Å as calculated for the conserved lysine residue of the Walker A motifs, which are shown as blue ribbons (Lys^{42} in MalK and Lys^{72} in OpuAA). As a consequence, the accessory domain of the second monomer of the OpuAA model (light grey) is displaced compared with the MalK structure (light magenta). A structural superimposition of the OpuAA model and the nucleotide-free semi-open form of MalK [20] revealed that one monomer imposes slightly less accurately with OpuAA (rmsd of 1.9 Å over 336 Cα atoms; results not shown). The Cα–Cα distance of opposing Walker A and ABC-signature motifs is also shorter (13 Å) than in the FRET-derived model of OpuAA (17 and 20 Å respectively).

Following the same strategy as outlined for the nucleotide-free state of OpuAA, a model was derived for the ATP-bound dimeric state (Figure 8A) that satisfied the distance restrains derived from

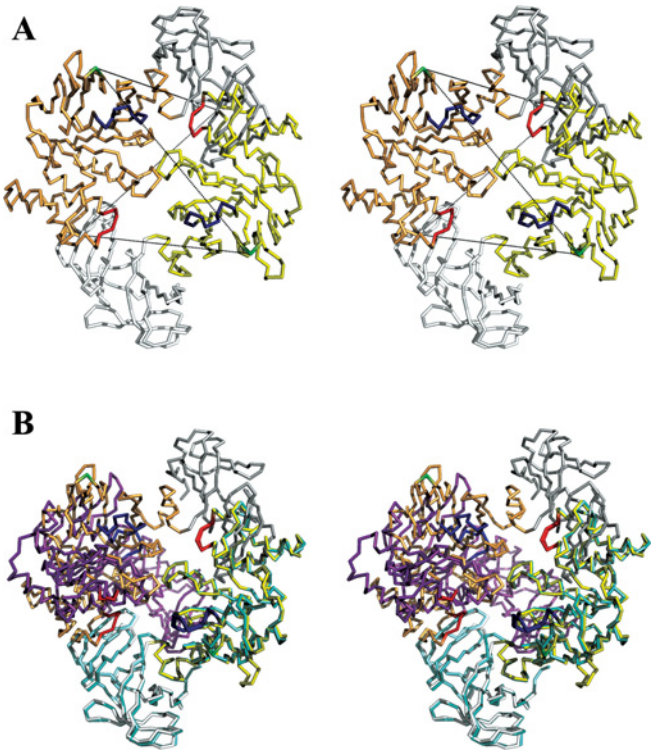

Figure 7 Stereo view of the FRET-derived homology model of nucleotide-free OpuAA

(**A**) The accessory domains are shown in white, whereas the canonical NBDs are given in yellow and light orange respectively. Note that the accessory domain of MalK was used in the homology modelling because proper location of the CBS domain, which is shown in Figure 1(C), is not possible. FRET-derived distances between amino acid residues 45 (green) and 161 (dark grey) are highlighted by black broken lines. The individual distances are given in Table 2. The Walker A motif is highlighted in blue and the ABC-signature motif in red. (**B**) Stereo view of a structural superimposition of the FRET-derived homology model of OpuAA and the open conformation of the nucleotide-free form of MalK (PDB entry: 1Q1E). Colour-coding of OpuAA is as in (**A**). Individual chains of MalK are shown in magenta and cyan, whereas the Walker A and ABC-signature motifs are highlighted in blue and red respectively. For structural superimpositions, the Walker A and B motifs were used. After improvement of the superimposition, the rmsd between monomer A of OpuAA and MalK was 1 Å over 381 Cα atoms.

FRET measurements in solution (Table 2). Here, the Cα–Cα distance between opposing Walker A and ABC-signature motifs shortens to 13 Å compared with the model of the nucleotide-free state. Furthermore, a superposition of the nucleotide-free and the ATP-bound state of the OpuAA model (Figure 8B) revealed that the canonical part of the NBD, coloured cyan and magenta, undergoes an induced fit upon ATP-binding, i.e. a rigid-body motion of the helical domain towards the catalytic domain.

DISCUSSION

The large body of biochemical data [39] and the crystal structures of MalK [20,21], the isolated NBD of the maltose transporter, combined with the recently published crystal structure of the full-length transporter [18], has provided a molecular picture of how substrate import is catalysed by this ABC importer. Thus a 'tweezers-like' motion was proposed for MalK. In this model, the additional domains of MalK form the bottom of the tweezers, keeping two MalK monomers together during the catalytic cycle, while the catalytic and helical domains of the MalK monomers undergo nucleotide-dependent association and dissociation reactions. A similar monomer–dimer equilibrium

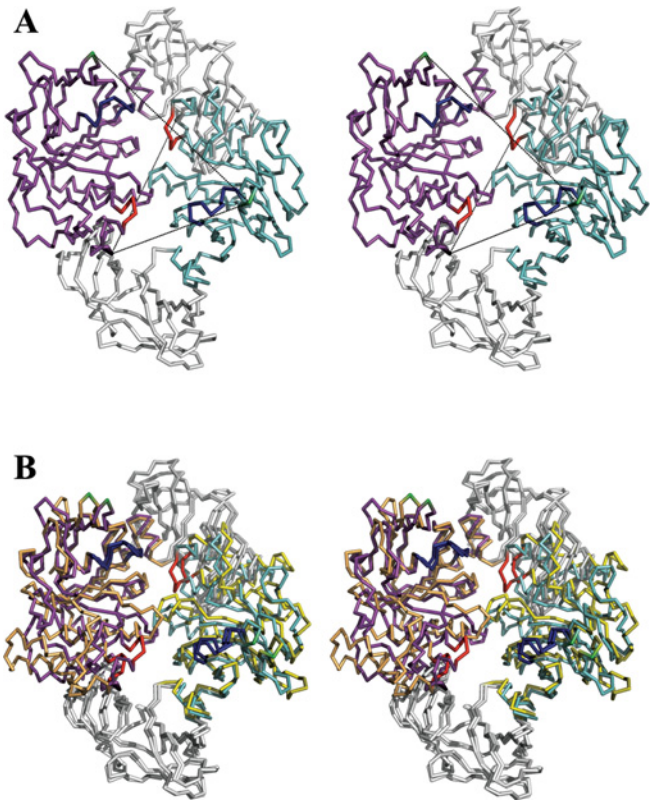

Figure 8 Stereo view of the FRET-derived homology model of OpuAA in the ATP-bound state

(**A**) ATP, which should be located between the Walker A (blue) and ABC signature (red) motifs of opposing monomers is not included in the model, because no structural knowledge of the exact position exists. The accessory domains, which adopt the structure of the MalK model, are depicted in white. The canonical NBDs are shown in cyan and magenta respectively. The anchors points (Ser^{45} and Gly^{161}), which were used in the FRET studies, are highlighted in green and black respectively and their distances are indicated by broken black lines (exact values are given in Table 2). (**B**) Stereo view of the structural superimposition of the FRET-derived homology models of OpuAA in the ATP-bound state (cyan and magenta) and the nucleotide-free state (yellow and light orange). Colour-coding of the conserved motifs is as in (**A**).

was observed for OpuAA from *B. subtilis* [11]. However, in contrast with MalK, dimeric OpuAA was only observed in the absence of nucleotides or the presence of ATP, although it remained monomeric in the presence of ADP. Moreover, dimeric OpuAA could be converted into the monomeric form in the presence of excess ADP. Such an ADP-induced monomerization of OpuAA, but not of MalK, might be due to differences in the accessory domains. In contrast with MalK, the primary structure of OpuAA indicates the presence of two CBS domains arranged in tandem (Figure 1). CBS domains are found, for example, in voltage-gated chloride channels [40] or IMPDHs [41] and are thought to bind small molecules containing an adenosyl moiety such as AMP, thereby regulating enzyme activity [42,43]. However, ATPase assays of OpuAA in the presence of AMP had no effect on activity and the stoichiometry of ATP (results not shown and [11]). This suggests that the CBS domains of OpuAA do not interact with AMP in a functionally relevant manner. Nevertheless, the core domain of MalK (catalytic and helical domain) is of sufficient homology (36 % identity and 69 % homology) with OpuAA to allow homology modelling (Figure 1), while a homology model of the accessory domain of OpuAA was constructed based on its closest structurally known homologue, TA0289 (Figure 1C). Based on this model, three amino acids were chosen and converted into cysteine residues (S45C, G161C and S171C) for subsequent fluorophore labelling.

Wild-type and the three mutant proteins could be overexpressed and purified to homogeneity (Supplementary Figure S1). As summarized in Table 1, turnover rates for the wild-type enzyme and the S45C and G161C mutants were identical within experimental error. Also the K_m values for the wild-type enzyme and the S45C were identical, whereas the K_m value for the G161C mutant increased by a factor of 5. The result is somewhat surprising since Gly^{161} is a surface-exposed residue and the structural model provides no explanation for this result. Since all subsequent experiments were performed under ATP-saturating conditions, these changes in K_m do not influence the results. In clear contrast, the S171C showed no ATPase activity and was not used in the following analysis.

Comparing this activity with the *in vivo* activity is not possible, because there exist no data on the number of transporters per cell [44]. However, assuming an activity typical for ATP transporters (approx. 1 ATP/s), indicates that the activity of the isolated NBD *in vitro* is 60 times lower than expected. But already in detergent solution, a 10-fold increase of the ATPase activity was observed in the presence of the TMD and the substrate-loaded SBP [9]. This clearly suggests that a properly assembled transporter requires higher activity than displayed by the isolated NBD. However, the results of the re-assembly studies in detergent solution [9] support the notion that the isolated NBD is properly folded and adopts a transport-competent state that can be stimulated in a SBP- and substrate-dependent manner.

The S45C and S161C were labelled employing two thiol-specific maleinimide fluorophores, OG and TR. The use of TR and OG, an efficient FRET pair [30] with a Förster radius of 51 Å, should in principle allow us to extract distance information in the different functional states of the isolated NBD, i.e. nucleotide-free, ATP- and ADP-bound. However, labelling efficiencies were at best 60 %, a result that cannot be explained based on the homology model, because the two residues chosen are surface-exposed. Instead of trying to optimize labelling efficiency, we developed an additional purification step to separate labelled and non-labelled species (Figure 2). Although the ion-exchange chromatogram indicated quantitative separation, we further analysed the identity and homogeneity of the two fractions obtained after ion-exchange chromatography by ESI–MS (Figure 3). Importantly, the amount of non-labelled OpuAA as indicated by an arrow in Figures 3(B) and 3(C) was below 2 % as calculated from the peak areas of the ESI–MS spectra of OpuAA S45C–OG and OpuAA S45C–TR respectively. These two independent sets of experimental evidence demonstrate a quantitative separation of labelled and non-labelled OpuAA, which is a prerequisite for subsequent quantitative FRET measurements.

A process to assemble and de-assemble homodimers of OpuAA has already been described in detail [11] and was readily applied to the labelled single cysteine mutants. However, FRET efficiency strongly depends on a complete donor–acceptor pairing [30]. Statistical mixing of a 1:1 mixture of OG- and TR-labelled OpuAA would in theory result in the formation of 25 % dimers composed of donors only (OG/OG), 25 % dimers composed of acceptors only (TR/TR) and 50 % composed of donor and acceptor (OG/TR). Although such statistical mixing has been verified experimentally for other isolated ABC-NBDs [37,45,46], and additionally a mathematical treatment to correct incomplete assembly is possible in principle, the dynamic monomer–dimer equilibrium of OpuAA would further complicate the evaluation. Therefore we decided to use a molar ratio of donor/acceptor of

1:9 to ensure quantitative 'pairing' of OpuAA–OG with OpuAA–TR. Under these conditions, FRET could be observed for the 45–45, 45–161 and 161–161 pairs in the nucleotide-free and ATP-bound state, but not in the ADP-bound state (Figure 4). Transfer efficiencies are summarized in Table 2. In the light of the biochemical characterization of the isolated NBD of the OpuA transporter [11], these results demonstrate that a dimer is present in the nucleotide-free and ATP-bound state respectively, whereas the protein is monomeric in the ADP-bound state. However, one has to realize that a determination of transfer efficiencies relies on an accurate protein concentration determination. Since the molar absorption coefficient of the dyes changed upon coupling (Supplementary Figure S2), protein concentration determination might become unreliable. To overcome, this problem, we also performed time-resolved FRET experiments (Figure 5). In this case, the decay in FRET signal of nucleotide-free or ATP-bound dimeric OpuAA samples was measured over time in the presence of 10 mM ADP, which induces dimer dissociation. From the determined amplitudes and the half time of dimer decay, transfer efficiencies could be calculated in a protein-concentration-independent way (Table 2). The agreement between these values and the values determined from the static measurements (Table 2) suggests that the distances, which can be derived from the transfer efficiencies, can be used as distance restrains for modelling the dimeric state of OpuAA.

Similarly to the HlyB system, the introduction of a tryptophan residue at position 19 of OpuAA lowered the catalytic efficiency of the enzyme 2-fold (Table 1). However, in our assays, saturating ligand concentrations were used and, more importantly, hydrolysis was prevented by adding EDTA to the buffer so that the enzymatic activity is not as important and the 2-fold reduction can be tolerated. Thus the chase of the nucleotide-free dimer of OpuAA F19W with ADP or ADP/Mg^{2+} displays the same result, as the ADP-induced dissociation of the OpuAA dimer detected by fluorescence, but FRET experiments report changes in distance, i.e. dimer decay directly, the F19W mutant uses nucleotide association/dissociation as the read-out. However, one has to keep in mind that the k_{cat} value of ATPase activity under these conditions is approx. 1 min^{-1} (Table 1 and [11]), whereas the half time of dimer decay was between 12.9 ± 0.1 and 22 ± 0.3 min. Stopped-flow experiments employing changes of the intrinsic tryptophan signal (results not shown) revealed that nucleotide association was faster than the time resolution of the experiment (approx. 1 ms). Thus ATPase activity is either limited by hydrolysis as suggested for the HlyB–NBD [28] or the dissociation of the dimer as suggested for MJ1276 [27]. The current model of ATP hydrolysis within ABC domains assumes that dimer decay occurs every time the two ATPs bound to the composite dimer are hydrolysed. Such a scenario is hard to imagine for OpuAA, because a k_{cat} of 1 min^{-1} and the half time of dimer decay (between 12 and 22 min) are not compatible with this model. However, Gadsby and co-workers [47] have demonstrated that, in CFTR (cystic fibrosis transmembrane conductance regulator), repetitive cycles of ATP hydrolysis can occur before the dimer decays. Clearly, in CFTR the NBD composite sites are unequal, because the degeneration of certain residues critical for catalysis generates one ATP-binding site with no or only little ATP activity, whereas the other site contains the canonical residues and is capable of hydrolysing ATP. Although OpuAA does not contain an asymmetrical ATP-binding site, it is tempting to speculate that the 10–20-fold difference between ATP turnover and dimer decay is due to a similar phenomena. ATP hydrolysis and dimer decay are not strictly coupled, and repetitive cycles can occur in both binding sites before the dimer dissociates. Dimer decay on the other hand would finally terminate ATPase activity. That would also suggest that a single ATP hydrolysis event and the overall termination of activity (dimer decay) might have different rate-limiting steps. However, this hypothesis requires further verification, and, although appealing, the differences between CFTR and OpuAA in sequence and the resulting functional consequences are obvious, therefore further experimental analysis is necessary before the discrepancy between turnover and dimer decay can be resolved.

Based on the distance restrains derived from the static and time-resolved FRET measurements (Table 2), the dimeric homology models of OpuAA (nucleotide-free and ATP-bound) that were based on the dimeric crystal structures of MalK, were modified to satisfy the restrains (Figures 7 and 8). As shown, in Figures 7(A) and 8(A), the FRET-derived distances can only be incorporated into the homology models if the accessory domains are not in close contact in OpuAA as they are in MalK. Furthermore, the catalytic and helical domains in the second monomer are translationally shifted by 9 Å if comparing MalK with OpuAA (Figure 7B). This excludes that a simple rotation of the linker between core NBD and the CBS-containing accessory domain is sufficient to generate a 'MalK-like' arrangement. However, one has to stress that the accessory domain of the OpuAA model shown in the present study contains the MalK-fold, whereas sequence analysis clearly revealed the presence of CBS domains in OpuAA that adopt a fold similar to the one shown in Figure 1(C). The low structural homology between these two folds prohibited any further homology modelling. Analysis of the buried surface area of the OpuAA model revealed a value of 130 $Å^2$ compared with 1900 $Å^2$ in the ATP-bound state of MalK [20]. Clearly, the calculated value of the buried surface area is too small to explain the dimeric nature of nucleotide-free OpuAA in solution [11]. However, the accessory domains, as shown in Figure 7(A), do not have any contact, so the only stabilization is provided by interactions of the canonical part (helical and catalytic domain) of OpuAA. Thus the FRET-derived model strongly suggests that the CBS-containing accessory domains stabilize the dimeric nature of this ATPase subunit, but that the relative orientation of canonical NBD and the accessory domain is different in OpuAA and MalK. This finding is similar to the situation observed in the crystal structure of CysA [48], the NBD of a putative sulfate-import system. In this case, the orientation of the accessory domain in one of the two dimers is also different from that of MalK and suggests that the relative three-dimensional orientation of the core NBD and the accessory domain is different in different NBDs and might be a consequence of functional requirements imposed on the transporter (nature of substrate, interacting molecules/proteins, etc.). On the other hand, a rigid-body inward motion is observed for the helical domain of the ATP-bound model compared with the nucleotide-free state (Figure 8B). This rigid-body motion of induced fit upon ATP-binding was first proposed for MJ1276 [49] and subsequently verified in the crystal structures of other isolated NBDs in the ATP-bound state [20,27–29]. Here, the inward motion ranged from 16° to 25°. In our model, the helical domain of the nucleotide-free state (coloured yellow and light orange in Figure 8B) undergoes an inward motion of approx. 17°. This demonstrates that the basic motion in the core NBD is also preserved in OpuAA.

In summary, although the orientation of the accessory domain is not identical in OpuAA and MalK, the basic principles of structural changes occurring within the helical domain upon ATP-binding that have been elaborated for many systems are also conserved in OpuAA. It is also tempting to speculate that the OpuAA dimer adopts the open conformation of MalK in solution in the absence of nucleotides and not the semi-open state, but with a different arrangement of the accessory domain

that very probably stabilizes the dimer and also performs a tweezer-like function as it was proposed for MalK [20]. Further studies, such as additional FRET or cysteine-based cross-linking experiments, are necessary to determine the exact orientation of the CBS domains to each other, but a definitive answer will only become available upon determining the three-dimensional crystal structure of OpuAA in different functional states. However, in the light of the proposed role of this module in regulating transport function, it is important to realize that not only the primary structure, but also the quaternary arrangement is important for *in vivo* function.

We thank Suman Lata, Jacob Piehler and all members of the Institute of Biochemistry for the stimulating discussions and Robert Tampé for constant support and encouragement. We are grateful to Filip Oesterhelt, Claus Seidel and Sander Smits for many insightful discussions concerning the FRET experiments and their interpretations. This work was supported by the DFG (special priority programme 1070, grants BR 796/51 to E. B. and Schm1279/4-1 to L. S.).

REFERENCES

1 Wood, J. M., Bremer, E., Csonka, L. N., Kraemer, R., Poolman, B., van der Heide, T. and Smith, L. T. (2001) Osmosensing and osmoregulatory compatible solute accumulation by bacteria. Comp. Biochem. Physiol. A Mol. Integr. Physiol. **130**, 437–460
2 Whatmore, A. M. and Reed, R. H. (1990) Determination of turgor pressure in *Bacillus subtilis*: a possible role for K^+ in turgor regulation. J. Gen. Microbiol. **136**, 2521–2526
3 Miller, K. J. and Wood, J. M. (1996) Osmoadaptation by rhizosphere bacteria. Annu. Rev. Microbiol. **50**, 101–136
4 Wood, J. M. (1999) Osmosensing by bacteria: signals and membrane-based sensors. Microbiol. Mol. Biol. Rev. **63**, 230–262
5 Ventosa, A., Nieto, J. J. and Oren, A. (1998) Biology of moderately halophilic aerobic bacteria. Microbiol. Mol. Biol. Rev. **62**, 504–544
6 Kempf, B. and Bremer, E. (1998) Uptake and synthesis of compatible solutes as microbial stress responses to high-osmolality environments. Arch. Microbiol. **170**, 319–330
7 Welsh, D. T. (2000) Ecological significance of compatible solute accumulation by micro-organisms: from single cells to global climate. FEMS Microbiol. Rev. **24**, 263–290
8 Minton, A. P. (2001) The influence of macromolecular crowding and macromolecular confinement on biochemical reactions in physiological media. J. Biol. Chem. **276**, 10577–10580
9 Horn, C., Bremer, E. and Schmitt, L. (2005) Functional overexpression and *in vitro* assembly of OpuA, an osmotically regulated ABC-transporter from *Bacillus subtilis*. FEBS Lett. **579**, 5765–5768
10 Schmitt, L. and Tampé, R. (2002) Structure and mechanism of ABC-transporters. Curr. Opin. Struct. Biol. **12**, 754–760
11 Horn, C., Bremer, E. and Schmitt, L. (2003) Nucleotide dependent monomer/dimer equilibrium of OpuAA, the nucleotide-binding protein of the osmotically regulated ABC transporter OpuA from *Bacillus subtilis*. J. Mol. Biol. **334**, 403–419
12 Horn, C., Sohn-Bosser, L., Breed, J., Welte, W., Schmitt, L. and Bremer, E. (2006) Molecular determinants for substrate specificity of the ligand-binding protein OpuAC from *Bacillus subtilis* for the compatible solutes glycine betaine and proline betaine. J. Mol. Biol. **357**, 592–606
13 Oswald, C., Holland, I. B. and Schmitt, L. (2006) The motor domains of ABC-transporters: what can structures tell us? Naunyn Schmiedebergs Arch. Pharmacol. **372**, 385–399
14 Dawson, R. J. and Locher, K. P. (2006) Structure of a bacterial multidrug ABC transporter. Nature **443**, 180–185
15 Locher, K. P., Lee, A. T. and Rees, D. C. (2002) The *E. coli* BtuCD structure: a framework for ABC transporter architecture and mechanism. Science **296**, 1091–1098
16 Pinkett, H. W., Lee, A. T., Lum, P., Locher, K. P. and Rees, D. C. (2007) An inward-facing conformation of a putative metal-chelate-type ABC transporter. Science **315**, 373–377
17 Hollenstein, K., Frei, D. C. and Locher, K. P. (2007) Structure of an ABC transporter in complex with its binding protein. Nature **446**, 213–216
18 Oldham, M. L., Khare, D., Quiocho, F. A., Davidson, A. L. and Chen, J. (2007) Crystal structure of a catalytic intermediate of the maltose transporter. Nature **450**, 515–521
19 Hvorup, R. N., Goetz, B. A., Niederer, M., Hollenstein, K., Perozo, E. and Locher, K. P. (2007) Asymmetry in the structure of the ABC transporter-binding protein complex BtuCD–BtuF. Science **317**, 1387–1390
20 Chen, J., Lu, G., Lin, J., Davidson, A. L. and Quiocho, F. A. (2003) A tweezers-like motion of the ATP-binding cassette dimer in an ABC transport cycle. Mol. Cell **12**, 651–661
21 Lu, G., Westbrooks, J. M., Davidson, A. L. and Chen, J. (2005) ATP hydrolysis is required to reset the ATP-binding cassette dimer into the resting-state conformation. Proc. Natl. Acad. Sci. U.S.A. **102**, 17969–17974
22 Panagiotidis, C. H., Boos, W. and Shuman, H. A. (1998) The ATP-binding cassette subunit of the maltose transporter MalK antagonizes MalT, the activator of the *Escherichia coli* mal regulon. Mol. Microbiol. **30**, 535–546
23 Bluschke, B., Volkmer-Engert, R. and Schneider, E. (2006) Topography of the surface of the signal-transducing protein EIIA(Glc) that interacts with the MalK subunits of the maltose ATP-binding cassette transporter (MalFGK2) of *Salmonella typhimurium*. J. Biol. Chem. **281**, 12833–12840
24 van der Heide, T. and Poolman, B. (2000) Glycine betaine transport in *Lactococcus lactis* is osmotically regulated at the level of expression and translocation activity. J. Bacteriol. **182**, 203–206
25 Bateman, A. (1997) The structure of a domain common to archaebacteria and the homocystinuria disease protein. Trends Biochem. Sci. **22**, 12–13
26 Biemans-Oldehinkel, E., Mahmood, N. A. and Poolman, B. (2006) A sensor for intracellular ionic strength. Proc. Natl. Acad. Sci. U.S.A. **103**, 10624–10629
27 Smith, P. C., Karpowich, N., Millen, L., Moody, J. E., Rosen, J., Thomas, P. J. and Hunt, J. F. (2002) ATP binding to the motor domain from an ABC transporter drives formation of a nucleotide sandwich dimer. Mol. Cell **10**, 139–149
28 Zaitseva, J., Jenewein, S., Jumpertz, T., Holland, I. B. and Schmitt, L. (2005) H662 is the linchpin of ATP hydrolysis in the nucleotide-binding domain of the ABC transporter HlyB. EMBO J. **24**, 1901–1910
29 Zaitseva, J., Oswald, C., Jumpertz, T., Jenewein, S., Wiedenmann, A., Holland, I. B. and Schmitt, L. (2006) A structural analysis of asymmetry required for catalytic activity of an ABC-ATPase domain dimer. EMBO J. **25**, 3432–3443
30 Lakowicz, J. R. (1999) Principles of Fluorescence Spectroscopy, Kluwer Academic Publishers, New York
31 Marti-Renom, M. A., Stuart, A. C., Fiser, A., Sanchez, R., Melo, F. and Sali, A. (2000) Comparative protein structure modeling of genes and genomes. Annu. Rev. Biophys. Biomol. Struct. **29**, 291–325
32 Laskowski, R. A., MacArthur, M. W., Moss, D. S. and Thornton, J. M. (1993) PROCHECK: a program to check the stereochemical quality of protein structures. J. Appl. Crystallogr. **26**, 283–291
33 Kleywegt, G. J. (1996) Use of non-crystallographic symmetry in protein structure refinement. Acta Crystallogr. Sect. D Biol. Crystallogr. **52**, 842–857
33a Collaborative Computational Project, Number 4 (1994) The CCP4 suite: programs for protein crystallography. Acta Crystallogr. Sect. D Biol. Crystallogr. **50**, 760–763
34 Schneider, E. (2001) ABC transporters catalyzing carbohydrate uptake. Res. Microbiol. **152**, 303–310
35 Diederichs, K., Diez, J., Greller, G., Muller, C., Breed, J., Schnell, C., Vonrhein, C., Boos, W. and Welte, W. (2000) Crystal structure of MalK, the ATPase subunit of the trehalose/maltose ABC transporter of the archaeon *Thermococcus litoralis*. EMBO J. **19**, 5951–5961
36 Berney, C. and Danuser, G. (2003) FRET or no FRET: a quantitative comparison. Biophys. J. **84**, 3992–4010
37 Zaitseva, J., Jenewein, S., Wiedenmann, A., Benabdelhak, H., Holland, I. B. and Schmitt, L. (2005) Functional characterization and ATP induced dimerization of the isolated ABC-domain of the haemolysin B transporter. Biochemistry **44**, 9680–9690
38 Jones, T. A., Zou, J. Y., Cowan, S. W. and Kjeldgaard (1991) Improved methods for binding protein models in electron density maps and the location of errors in these models. Acta Crystallogr. Sect. A Found. Crystallogr. **47**, 110–119
39 Davidson, A. L. and Chen, J. (2004) ATP-binding cassette transporters in bacteria. Annu. Rev. Biochem. **73**, 241–268
40 Meyer, S. and Dutzler, R. (2006) Crystal structure of the cytoplasmic domain of the chloride channel CIC-0. Structure **14**, 299–307
41 Zhang, R., Evans, G., Rotella, F. J., Westbrook, E. M., Beno, D., Huberman, E., Joachimiak, A. and Collart, F. R. (1999) Characteristics and crystal structure of bacterial inosine-5′-monophosphate dehydrogenase. Biochemistry **38**, 4691–4700
42 Bennetts, B., Rychkov, G. Y., Ng, H. L., Morton, C. J., Stapleton, D., Parker, M. W. and Cromer, B. A. (2005) Cytoplasmic ATP-sensing domains regulate gating of skeletal muscle CIC-1 chloride channels. J. Biol. Chem. **280**, 32452–32458
43 Scott, J. W., Hawley, S. A., Green, K. A., Anis, M., Stewart, G., Scullion, G. A., Norman, D. G. and Hardie, D. G. (2004) CBS domains form energy-sensing modules whose binding of adenosine ligands is disrupted by disease mutations. J. Clin. Invest. **113**, 274–284
44 Kempf, B. and Bremer, E. (1995) OpuA, an osmotically regulated binding protein-dependent transport system for the osmoprotectant glycine betaine in *Bacillus subtilis*. J. Biol. Chem. **270**, 16701–16713
45 Janas, E., Hofacker, M., Chen, M., Gompf, S., van der Does, C. and Tampe, R. (2003) The ATP hydrolysis cycle of the nucleotide-binding domain of the mitochondrial ATP-binding cassette transporter Mdl1p. J. Biol. Chem. **278**, 26862–26869

46 Nikaido, K. and Ames, G. F. (1999) One intact ATP-binding subunit is sufficient to support ATP hydrolysis and translocation in an ABC transporter, the histidine permease. J. Biol. Chem. **274**, 26727–26735

47 Vergani, P., Lockless, S. W., Nairn, A. C. and Gadsby, D. C. (2005) CFTR channel opening by ATP-driven tight dimerization of its nucleotide-binding domains. Nature **433**, 876–880

48 Scheffel, F., Demmer, U., Warkentin, E., Hulsmann, A., Schneider, E. and Ermler, U. (2005) Structure of the ATPase subunit CysA of the putative sulfate ATP-binding cassette (ABC) transporter from *Alicyclobacillus acidocaldarius*. FEBS Lett. **579**, 2953–2958

49 Karpowich, N., Martsinkevich, O., Millen, L., Yuan, Y. R., Dai, P. L., MacVey, K., Thomas, P. J. and Hunt, J. F. (2001) Crystal structures of the MJ1267 ATP binding cassette reveal an induced-fit effect at the ATPase active site of an ABC transporter. Structure **9**, 571–586

Received 22 October 2007/5 March 2008; accepted 6 March 2008
Published as BJ Immediate Publication 6 March 2008, doi:10.1042/BJ20071443